



Behavior of Nb influence on structure and properties of 30Cr13 cast martensitic stainless steel

Yang-fan Jin¹ · Tuo Zhang¹ · Qi-yu Zang¹ · Yi-tao Yang¹

Received: 5 April 2018 / Revised: 1 November 2018 / Accepted: 8 November 2018 / Published online: 26 November 2018
© China Iron and Steel Research Institute Group 2018

Abstract

The microstructure, mechanical properties and corrosion resistance of 30Cr13 martensitic stainless steel (MSS) with different Nb contents were investigated by using the optical microscope, scanning electron microscope, X-ray diffractometer, HRC hardness measurement apparatus and tensile testing machine. Nb was found to retard the formation of austenite and promote the precipitation of carbides by calculating. The results showed that the addition of 0.2 wt.% Nb elements could improve the strength and corrosion resistance of 30Cr13 martensitic stainless steels while the reduction in toughness was less because of the inhibited effect on Cr-rich carbides precipitation by Nb addition. Specially, $M_{23}C_6$ -type carbides almost disappeared in 0.6Nb-MSS. Moreover, the main existent form of Nb element was NbC and the strong carbide-forming ability of Nb element increased the quantity of carbides with the morphology changing from spherical-type to chain-type. 0.2Nb-MSS shows excellent strength, adequate toughness and sufficient corrosion resistance for the application.

Keywords Niobium addition · Martensitic stainless steel · Microstructure · Mechanical property · Corrosion resistance

1 Introduction

Martensitic stainless steels (MSSs) have been increasingly applied in aerospace, medical equipment, mold industry and military industry owing to the preferable combination of mechanical properties and corrosion resistance [1, 2], and MSSs with high carbon content are also used in tool production. This kind of material can be strengthened by heat treatment, alloying and work-hardening, etc. According to the different contents of carbon, MSSs can be divided into three groups, and 30Cr13 steel belongs to medium carbon MSS. 30Cr13 MSSs possess higher hardness, better wear and corrosion resistance and are widely used in production of the plastic injection molds [3, 4]. However, the trend of lightweight has higher requirements of MSSs, which means that it is necessary to improve the mechanical properties of MSSs to achieve the goal of lightweight [5, 6]. At present, it is a possible way to strengthen MSSs

by adding N and Si elements, but the effect is not quite satisfactory. For example, it is easy for N element to escape from the molten steel and the addition of N element will deteriorate the toughness sharply because of the precipitation of rod-type Cr_2N [7, 8].

Some studies [9, 10] on Nb micro-alloying of ferritic stainless steel, austenitic stainless steel and die steel have shown that Nb as a ‘stabilizing and refining element’ raises strength and toughness effectively. MC-type carbide which is Nb-rich in Nb micro-alloyed steels can play the role of the secondary hardening [11, 12] and Nb element can refine the carbide to improve wear resistance and toughness [13, 14]. However, a high Nb addition has a pernicious effect on toughness because the network-type carbide precipitated at grain boundary will prevent the transmission of plastic deformation and Nb-rich carbides are stable at high temperature even at 1100 °C [15–17]. In other words, a critical Nb content exists which is beneficial to mechanical properties. However, compared to austenitic or ferritic stainless steels, investigations on the microstructure, mechanical properties and corrosion resistance of Nb bearing MSSs were rarely carried out, especially the studies on the corrosion resistance. Therefore, it is the

✉ Yi-tao Yang
yangyitao@shu.edu.cn

¹ School of Materials Science and Engineering, Shanghai University, Shanghai 200444, China

innovation point to add Nb element into MSSs. In this paper, the contents of carbides in MSSs can be accurately measured by electrolytic extraction experiment, and the type of carbides can be analyzed conveniently. A series of MSSs with different Nb contents have been designed to investigate the effect of Nb element on phase transformation, microstructure, mechanical properties and corrosion resistance, which benefit from four experimental steel.

2 Experimental

The experimental alloys were melted in a laboratory high-vacuum electric arc furnace using pure iron, pure chromium, pure manganese, 45 carbon steel, 65NbFe and 75SiFe master alloys as the raw materials, while the melting procedure was conducted with the protection of argon atmosphere. The chemical compositions analyzed by direct reading spectrometry (PMI-MASTER PRO) are shown in Table 1. The homogenizing treatment temperature was set at 1100 °C for 2 h to reduce the composition segregation, and then, the alloys were austenitized at 1050 °C for 0.5 h, followed by water quenching. Finally, tempering temperature was set to be 420 °C for 2 h and the alloys were cooled in air until room temperature. Microstructure and mechanical properties of cast alloys could be improved by heat treatment.

The samples were machined by wire cut electrical discharge machining into the dimension of 10 mm × 10 mm × 5 mm, 10 mm × 10 mm × 10 mm and 10 mm × 10 mm × 3 mm for microstructure characterization, electrolytic extraction experiment and corrosion measurement, respectively. Picric acid reagent was used as the etchant for microstructure observation before being characterized by optical microscopy (OM, Nikon LV150) and scanning electron microscopy (SEM, HITACHI SU-1500).

The mechanical properties were evaluated by hardness and tensile tests. Hardness was determined by HRC hardness measurements (HBE-3000A), and the tensile tests were performed on a tensile testing machine (CMT5105) with an extensometer at strain rate of 2 mm/min.

Table 1 Chemical composition of tested steels with different Nb contents (mass%)

No.	C	Cr	Mn	Si	Nb	Fe
1—0 wt.% Nb	0.303	13.9	0.349	1.49	—	Balance
2—0.2 wt.% Nb	0.319	13.0	0.338	1.63	0.204	Balance
3—0.4 wt.% Nb	0.291	13.1	0.342	1.64	0.354	Balance
4—0.6 wt.% Nb	0.310	13.0	0.392	1.62	0.761	Balance

The content and category of carbides were measured by electrolytic extraction experiment and X-ray diffraction (XRD, 18KW D/MAX2500V+/PC), respectively. The electrolyte consisted of analytical pure $C_6H_8O_7 \cdot H_2O$, HCl and deionized water. The experiment lasted for 8 h. The weight before and after test of each sample and the extraction production after drying were measured, among which the weighing was conducted via an electronic analytical balance with precision of 0.0001 g. The extraction production was analyzed by X-ray diffraction using $Cu-K\alpha$, scanning range from 10° to 90° at a scan rate of 4 (°)/min.

The immersion corrosion tests were performed at room temperature for 12 h, and 6 wt.% $FeCl_3$ solution was composed of analytically pure $FeCl_3 \cdot 6H_2O$ with deionized water as corrosion medium. The surface area and the weight before test of each sample were measured. After tests, each sample was rinsed by running water and the corrosion products were cleaned by tools. Then, the tested samples were flushed by alcohol and dried, followed by weighing again.

3 Results and discussion

3.1 Phase transformation

The equilibrium phase diagrams of the steels were calculated by JMatPro software, as shown in Table 2. With the increasing content of Nb, the proportion of both α -Cr and $M_{23}C_6$ -type carbides gradually increased while the proportion of M(C, N)-type carbide decreased. As one of the strong carbide-forming elements, Nb addition to MSS was desirable for thermodynamic potential for precipitation of NbC would be lowered, which would avoid the precipitation of Cr-rich $M_{23}C_6$ -type carbide. Then, the content of Cr in matrix would reach a relatively high level, making it possible for α -Cr to nucleate. However, α -Cr phase usually exists in high-temperature alloys with the content of Cr higher than 16% [18, 19]. Therein, whether α -Cr exists in the experimental alloys has to be detected.

Table 2 Equilibrium phases in tested steel calculated by JMatPro

Nb/wt.%	Ferrite/%	$M_{23}C_6$ /%	α -Cr/%	M(C, N)/%
0	86.3	5.5	8.2	0
0.2	86.1	5.1	8.6	0.2
0.4	85.9	4.7	9	0.4
0.6	85.7	4.2	9.4	0.7

Nb, as the ferrite forming element, has the effect of extending the area of ferrite phase while reducing that of austenite [20]. In order to quantitatively analyze the effect of Nb on phase transformation, results calculated by JMatPro are shown in Fig. 1. With the increase in content of Nb, the high-temperature ferrite phase region was enlarged and the formation of austenite was delayed correspondingly. Consequently, the temperature of homogenizing and austenitizing treatment has been set between 900 and 1200 °C to avoid the high-temperature ferritic nucleation. As a result, 1100 °C and 1050 °C were regarded as diffusion annealing and austenitizing temperatures, respectively.

3.2 Microstructural characterization

Figure 2 shows OM image of highly dislocated lath martensite with a small amount of carbides in MSS and Nb-MSS. As shown in Fig. 2a–c, the morphology of 0Nb-MSS and 0.2Nb-MSS was the branch crystal, while the branch of 0Nb-MSS was longer than that of 0.2Nb-MSS. The same morphology could not be observed in the other two samples, which means that branch morphology could be caused by Nb addition.

In Fig. 2d, e, original austenite grain boundaries became apparent in MSS samples with high Nb content as carbides precipitated along the boundaries. These carbides strongly inhibited the growth of original austenite. With the increase in Nb content, the precipitation of carbides was promoted and the carbide type changed from spherical-shape to rod-shape, and finally network-shape. Some black phases appeared on the edges of the carbides in samples with high Nb content.

As mentioned before, the precipitates mainly located at the grain boundaries. In Fig. 3a, there was no obvious

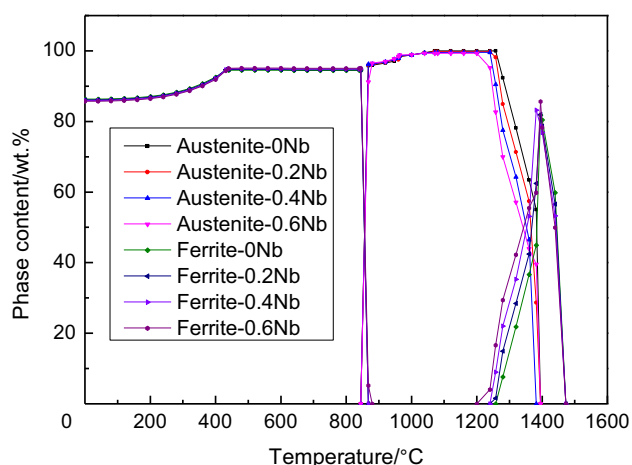


Fig. 1 Contents of austenite and ferrite in tested steel calculated by JMatPro

accumulation of carbides, and the carbides were mainly dispersively distributed in the martensite plate, which plays a role of dispersion strengthening. It could be found in Fig. 3b–d that the carbides had a trend to aggregate into chains. Short rod-type carbides grew into long chain-type with higher Nb addition. In Fig. 3c, d, a small amount of irregular shape phase could be observed, which is consistent with black phase in OM images.

According to energy-dispersive spectrometer (EDS) spectrum, all carbides in these samples belonged to Fe–Cr–C system. The carbides in Nb-MSSs also belonged to Nb–Fe–Cr–C system owing to strong carbide-forming ability of Nb. The black phases with irregular shape were combined with Fe and Cr elements, where a large amount of carbides distributed. Nb element promoted the precipitation of carbides, causing the carbon-depleted regions around carbides, and it was likely for Fe–Cr phase to form in these regions since carbon in solid solution prevented the formation of Fe–Cr phase due to its inability to dissolve carbon. With lowering carbon content to a critical minimum concentration of nucleation of Fe–Cr phase, Fe–Cr phase nucleated besides carbides, and subsequently Fe–Cr phase nucleus grew up to Fe–Cr phase particles through a diffusion of Cr element from Cr-rich carbides and matrix [21], which was a little different between experimental results and simulated calculation.

Figure 4 shows the analysis results of branch-type morphology in Fig. 2. The mapping scan shows the distribution of Cr, Fe, Si and C elements. Fe and C elements had no obvious relation with branch-type morphology. The distribution of Si and Cr elements was related to the morphology of dendrites. The light-colored regions in SEM image contained higher Cr and Si elements. Due to the segregation of Cr elements, the region could resist the corrosive agent and form the dendritic morphology. At the same time, carbides were mainly distributed in the light-colored regions and the formation of precipitation was related to the high content of Cr elements.

3.3 Carbides

Carbide content was evaluated by the weight-loss method in an electrolytic extraction experiment. The measured results showed that the carbide content in the samples also increased with the increase in Nb content (Fig. 5). Carbide content increased from 0.604 to 1.600% with the addition of up to 0.6 wt.% Nb, which was in an agreement with observed microstructure. By the way, with the increase in the content of Nb element, carbides precipitation rate was accelerated. The solubility of NbC in molten steel was generally presented in terms of weight percentages of the related elements in the solubility products. NbX (X = C or N and X is C in this paper) can form when the contents of

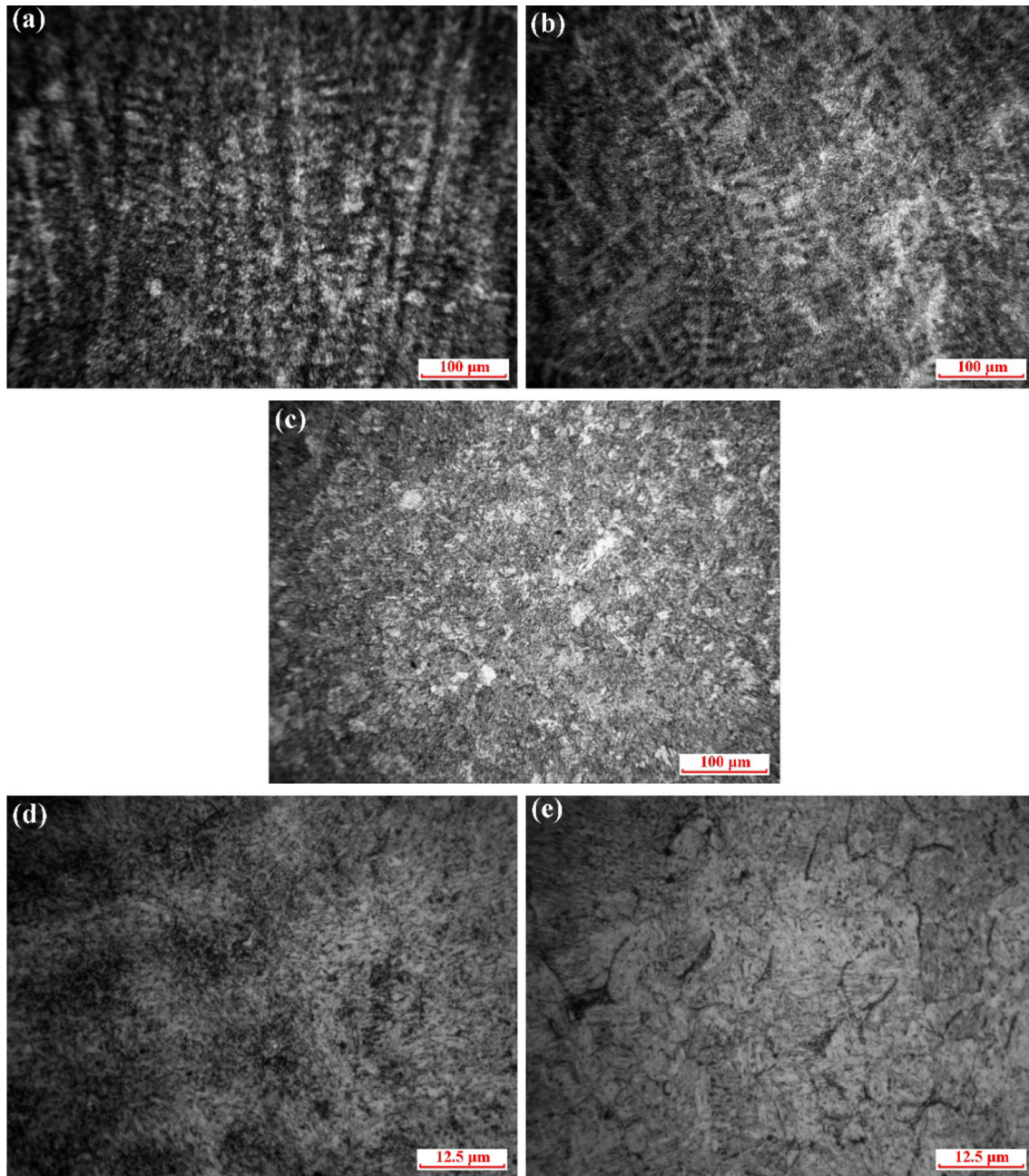
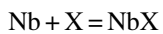


Fig. 2 Metallographic photographs of samples with different contents of Nb. **a** 0 Nb; **b, d** 0.2 wt.% Nb; **c** 0.4 wt.% Nb; **e** 0.6 wt.% Nb

Nb and nonmetallic element X are higher than the equilibrium values. The reaction between Nb and X in molten steel is written as Eq. (1) [22].



$$-\log K_{\text{NbX}} = \log E_S + \log f_{\text{Nb}} + \log f_X = B - \frac{A}{T} \quad (1)$$

where K_{NbX} is the equilibrium constant for the reaction from Eq. (1); E_S is the equilibrium solubility product for NbX formation in the steel; f_{Nb} and f_X are the activity coefficients of Nb and X, respectively; A and B are the constants; and T is the absolute temperature.

It could be clearly seen from Eq. (1) that, as Nb content increased, equilibrium absolute temperature rose. As a result, the carbides could start to precipitate at a high temperature and have enough time to grow up. Moreover, as Nb is a strong carbide-forming element, higher Nb content could remove more C elements from matrix to form MC-type carbides. Therefore, electrolytic extraction experiments and metallographic microstructure observations had reached the same conclusion that the tendency of carbide content was consistent with the content of Nb elements.

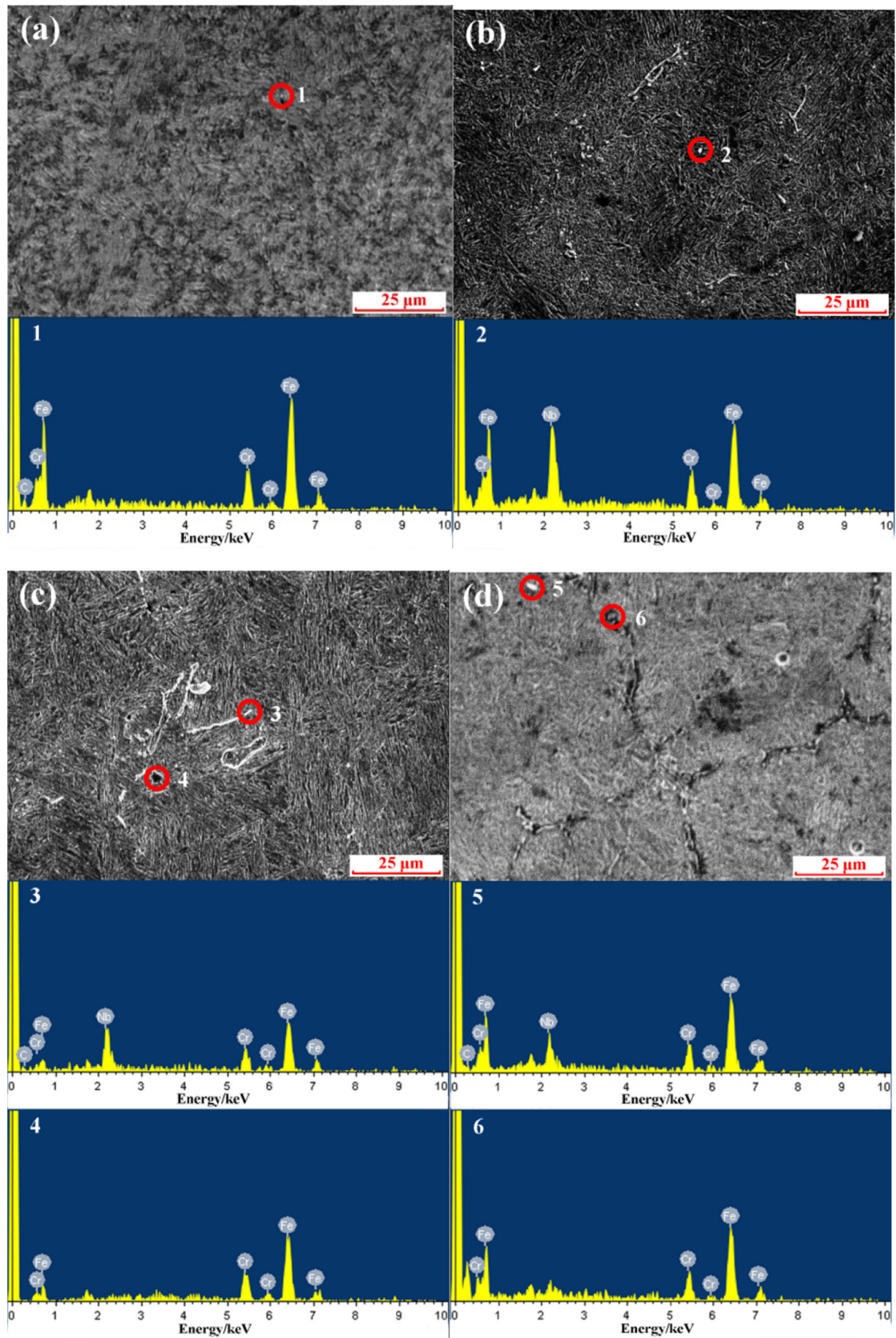


Fig. 3 SEM image and EDS analysis of samples with different contents of Nb. **a** 0 Nb; **b** 0.2 wt.% Nb; **c** 0.4 wt.% Nb; **d** 0.6 wt.% Nb

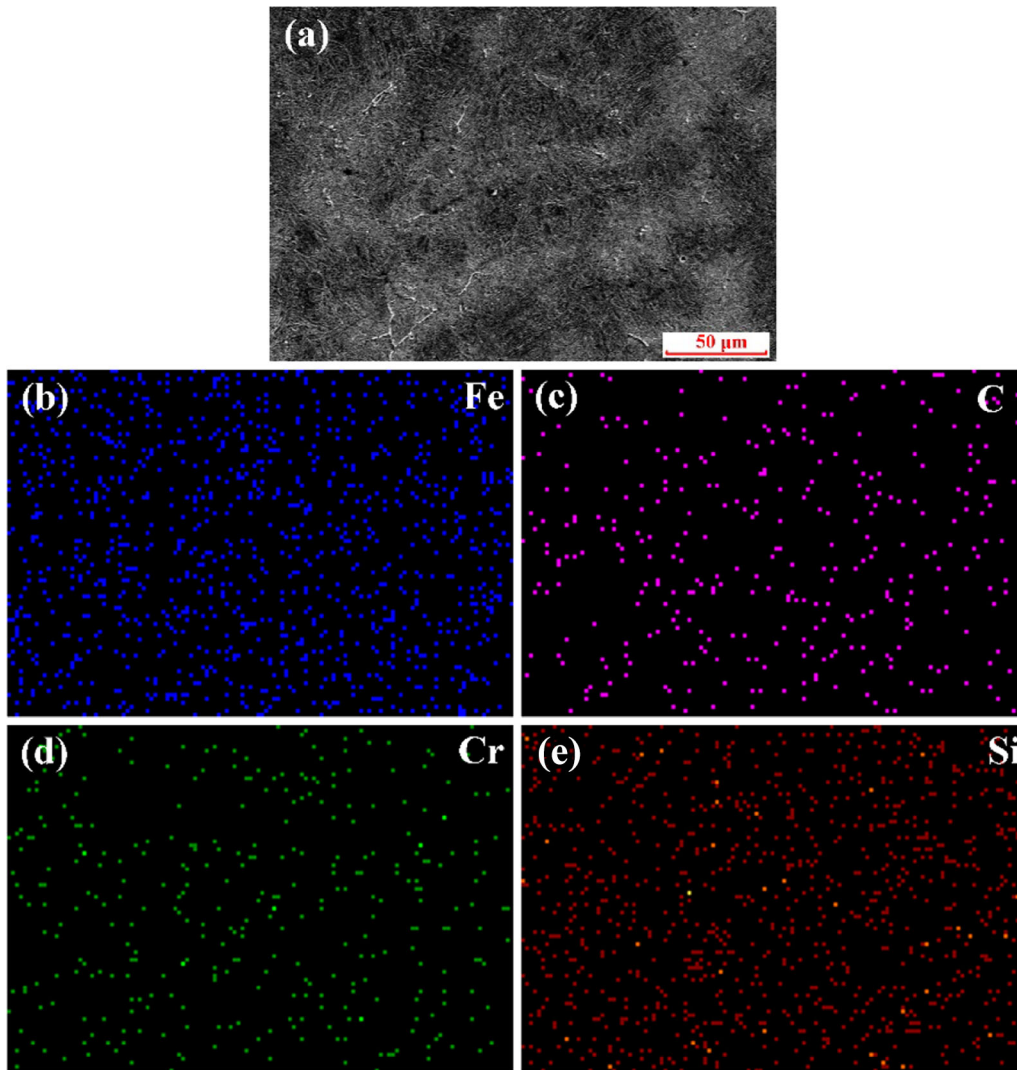


Fig. 4 EDS analysis of samples with addition of 0.2 wt.% Nb

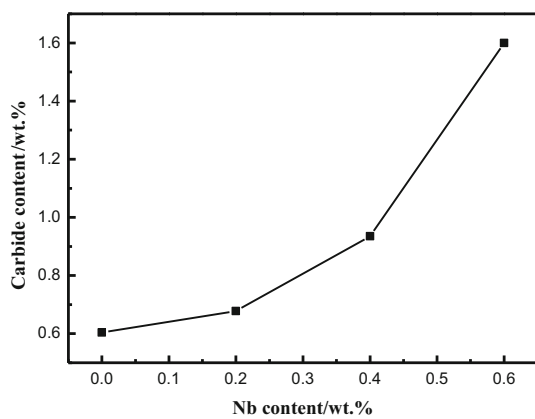


Fig. 5 Statistical analysis of quantity of carbides

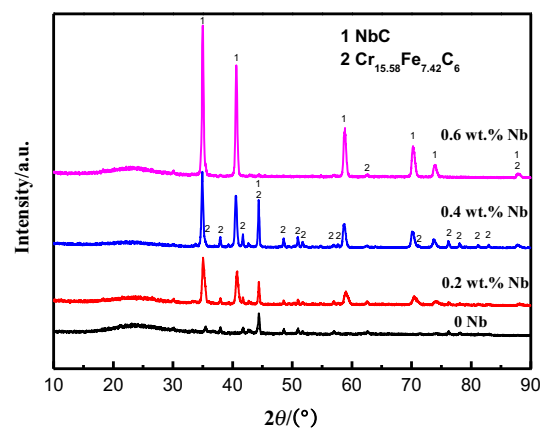


Fig. 6 X-ray diffraction pattern of carbides

XRD pattern of carbides in samples with different Nb contents is shown in Fig. 6. The carbides changed from single Cr_{15.58}Fe_{7.42}C₆ to the combination of NbC and

Cr_{15.58}Fe_{7.42}C₆ with the Nb addition. Furthermore, the intensity of NbC diffraction peak increased with Nb

content. When Nb content reached 0.6 wt.%, it could be observed in Fig. 6 that the diffraction peak of $\text{Cr}_{15.58}\text{Fe}_{7.42}\text{C}_6$ almost disappeared while that of NbC diffraction reached the maximum. The results of X-ray diffraction were consistent with those of microstructure observation and EDS energy spectrum analysis. Nb has stronger binding ability with C element than with Cr element. With the increase in Nb content, carbides will gradually transform from Cr-rich carbides to Nb-rich carbides.

Percentage of M_{23}C_6 -type and MC-type carbides in samples with different Nb contents is listed in Table 3. Even in the sample with 0.2 wt.% Nb, the composition ratio of carbides also changed greatly. The percentage of NbC carbides reached 33.9% in 0.2Nb-MSS sample, and with the increase in Nb content, it increased to 66.7% and 96.1%. Furthermore, M_{23}C_6 -type carbide nearly disappeared in 0.6Nb-MSS sample. Table 3 shows the ratios of carbides in 0.2Nb- and 0.4Nb-MSS sample that are basically similar, while the total carbide contents in 0.4Nb-MSS sample were more than those in 0.2Nb-MSS sample and the carbide aggregated into chains. It provided a favorable condition for the nucleation of Fe–Cr phase in the closed and carbon-depleted regions formed by carbide chain. The changes in phase quantity were consistent with the calculation results.

3.4 Mechanical properties

The macroscopic hardness measurement results of the as-cast and tempered samples are shown in Fig. 7, which were maintained near (56.2 ± 0.2) HRC. Considering the measurement error, the macroscopic hardness of the four samples was considered to be similar. After quenching and tempering treatment, the macroscopic hardness of the samples decreased with the increase in Nb content. Combined with the microstructure observation and carbides contents, the decrease in hardness was mainly because the carbides precipitate along grain boundary into chains and the dispersion strengthening effect was not obvious. With the increase in Nb content, carbide gathered together more obviously, and thus, C content in the matrix is lower. As is known that C content is the primary factor influencing the martensite hardness, the hardness declines with Nb content increasing. The hardness of the as-cast samples was basically close because the cast samples were cooled in a vacuum melting furnace which means different cooling

Table 3 Percentage of M_{23}C_6 -type and MC-type carbides

Nb content/wt.%	0	0.2	0.4	0.6
$\text{M}_{23}\text{C}_6/\%$	100	33.9	33.0	3.9
MC/%	0	66.1	67.0	96.1

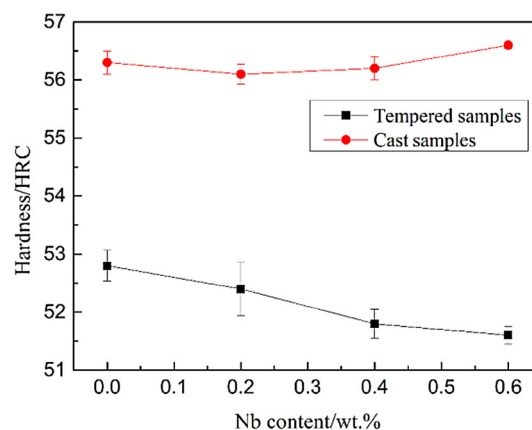


Fig. 7 Variations of hardness with Nb content in as-cast and tempered samples

rates. The as-cast samples were cooled faster, so that the precipitates have not enough time to grow up, resulting in the hardness slightly higher than that of the tempered samples.

The samples of tensile test were nonstandard samples, with a gauge length of 10 mm, width of 4 mm and thickness of 1 mm. The strain rate is 2 mm/min. Tensile strength and elongation characterized the toughness and strength of the material. Figure 8 shows that the tensile strength increases first and then decreases with the increase in Nb content, and the tensile strength reached a peak of 1714.1 MPa with Nb addition of 0.2 wt.%. The main strengthening mechanisms of Nb element were solid solution strengthening and precipitation strengthening. Amounts of carbides could be observed in 0.2Nb-MSS, whose size was significantly greater than that in 0Nb-MSS. Though main short rod-type carbides distributed in grain boundary, some of them still distributed in martensitic matrix to play the role of dispersion strengthening effect and improve the tensile strength. With further increase in Nb content, the tensile strength decreased gradually and reached the lowest value of 1525.4 MPa (0.6Nb-MSS). In

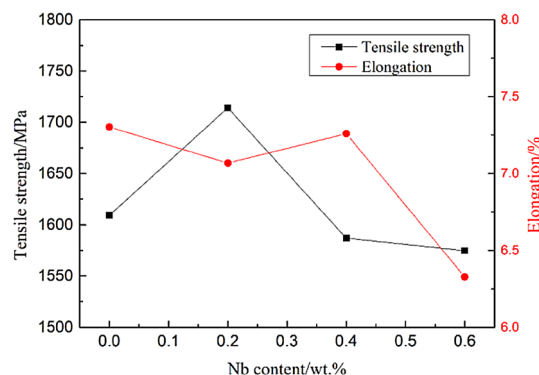


Fig. 8 Variations of tensile strength and elongation with Nb content in samples

0.4Nb-MSS and 0.6Nb-MSS samples with chain-type carbides on grain boundary, C content in matrix reduced and so was the tensile strength. The elongation first decreased and then increased, finally decreased again. In addition, it was usual for toughness reduced while the tensile strength had been enhanced. In 0.2Nb-MSS, the carbide content was higher than that in 0Nb-MSS, and carbides with oval-round shape mainly precipitated on dislocation, grain boundary and sub-boundary. The carbides could effectively pin the movement of dislocation and have significant effect on increasing the strength. The plastic deformation was difficult to transfer and caused toughness of 0.2Nb-MSS to decrease. The toughness was mainly influenced by the toughness of the matrix and the morphology of carbides. With the increase in Nb content, the numbers of precipitation increased, C content of matrix was reduced and toughness of martensitic matrix would be improved. At the same time, as the carbides gathered in grain boundary, leading to stress concentration, micro-cracks would be easily formed under loads. The matrix toughness of 0.4Nb-MSS increased more than the stress concentration caused by carbides. As a whole, the toughness was improved. However, a large number of network-type carbides in 0.6Nb-MSS result in more serious stress concentration, and then, elongation began to decline even though the toughness of matrix was improved. 0.2Nb-MSS exhibits tensile strength of 1714 MPa, 30% higher than 0Nb-MSS. Elongation was around 7% (reduced by 3.2%). Therefore, Nb element could strengthen the martensitic stainless steel with a small toughness loss.

In order to accurately analyze the influence of Nb elements on the fracture mode, SEM is used to observe the fracture of samples after tensile tests, as shown in Fig. 9. The fracture morphology was similar with small difference: it was complex fracture combining brittle and ductile fracture characteristics. There were a large number of small toughening nests distributed on fracture. Before fracture, a certain degree of plastic deformation happened, resulting in great tensile strength during tensile process, which was in conformity with the results of tensile experiments. As shown in Fig. 9, there were a large number of small holes distributed diffusely, and some small size cleavage platforms with tearing ridge and micro-cracks on it. It could be found in Fig. 9a–c that these small holes with greater depth of field were considered to be toughening nests. The cleavage platform in 0.6Nb-MSS was more obvious than that in the other three samples. The size of the cleavage platform was larger and the shape of the hole had been changed. The cleavage platform in Fig. 9d showed a stepped distribution, and there were some round holes. The sample was inclined to brittle fracture, which was consistent with the elongation measurement results.

3.5 Corrosion resistance

Corrosion resistance was measured by immersion corrosion test in 6 wt.% FeCl₃ solution at room temperature for 12 h. Experimental steels all had different corrosion morphologies on the surface with variation of Nb contents. As shown in Fig. 10, the corrosion behavior of 0Nb-MSS and 0.2Nb-MSS samples was similar, which began with a single corrosion point and gradually expanded to the macro-morphology exhibited in Fig. 10a, b. However, a large amount of Cr-rich carbides caused several chromium-depleted regions, while more weak area of passivation layers made corrosion points bigger on size and much more on number.

The parameters measured by immersion corrosion tests are listed in Table 4. The corrosion resistance of experimental steels was characterized by mass loss (V), which can be defined as [23]:

$$V = \frac{M - m}{St} \quad (2)$$

where M and m are the weight before and after test, respectively; S is the surface area of specimen; and t is the time of corrosion test.

Figure 11 shows the corrosion rate after immersion corrosion test in 6 wt.% FeCl₃ solution at room temperature for 12 h. The corrosion rate of 0Nb-MSS was 0.01662 mg mm⁻² h⁻¹, while that of 0.2Nb-MSS dropped significantly to 0.01313 mg mm⁻² h⁻¹. With increase in Nb content, the corrosion rate increased to 0.01763 and 0.01753 mg mm⁻² h⁻¹, which was considered to be the same by considering the experimental error. Nb addition could dramatically improve the corrosion resistance of the designed MSSs. Nevertheless, more Nb addition led to a negative effect on the corrosion rate. In other words, there was a critical Nb content most beneficial to corrosion resistance. Nb element in Nb-MSSs inhibits the formation of Cr-rich carbides, and thus, Cr content in matrix reached a high level. As is known, Cr is the main element affecting the corrosion resistance of stainless steel, leading to improvement in the corrosion resistance of 0.2Nb-MSS. Though 0.4Nb-MSS and 0.6Nb-MSS samples contained less M₂₃C₆-type carbides, the nucleation and growth of Fe–Cr phase consumed quantities of Cr elements, resulting in the form of chromium-depleted regions. The passivation film formed over chromium-depleted regions would lack enough Cr element to form a new passive film if the existing film was destroyed by external environment. Thus, the corrosion resistance got worse. Based on the above theory, no evident chromium-depleted regions existed in 0Nb-MSS and 0.2Nb-MSS while several existed in 0.4Nb-MSS and 0.6Nb-MSS, which caused the different macro-

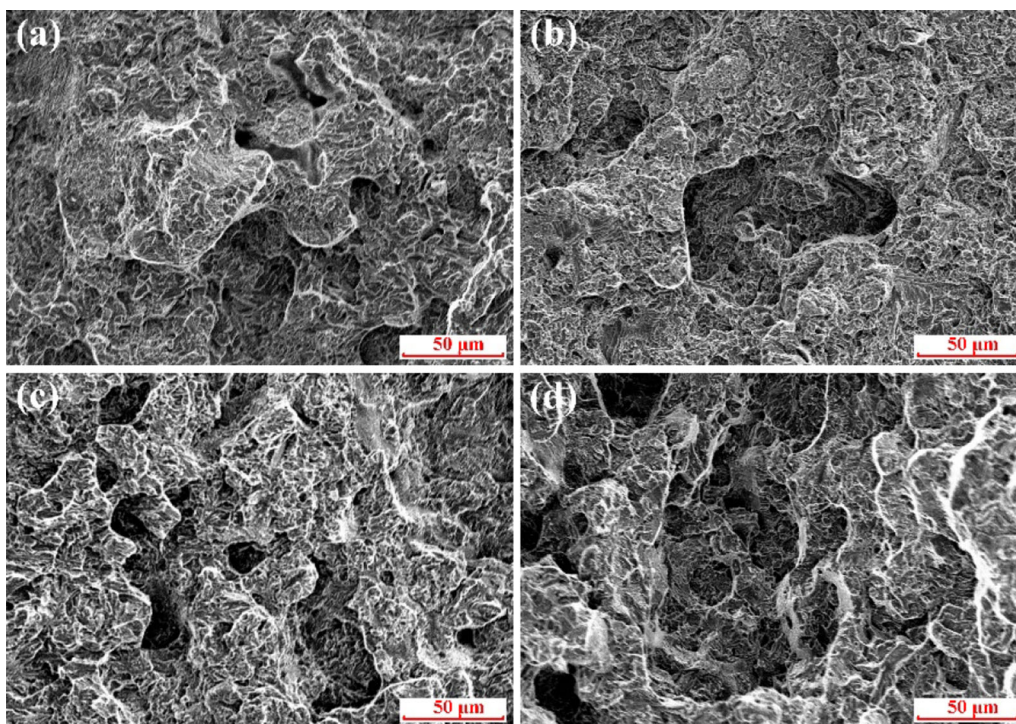


Fig. 9 SEM fracture morphology of samples with different Nb contents. **a** 0 wt.%; **b** 0.2 wt.%; **c** 0.4 wt.%; **d** 0.6 wt.%

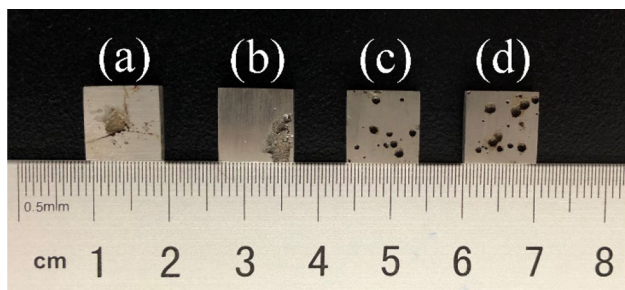


Fig. 10 Macromorphology of samples after immersion corrosion test at room temperature for 12 h in 6 wt.% FeCl_3 solution. **a** 0Nb-MSS; **b** 0.2Nb-MSS; **c** 0.4Nb-MSS; **d** 0.6Nb-MSS

Table 4 Parameters of immersion corrosion

No.	Nb content/wt.%	M/mg	m/mg	S/mm^2	t/h
1	0	2194.7	2130.4	322.4	12
2	0.2	2163.5	2113.5	317.4	12
3	0.4	2157.1	2090.1	316.9	12
4	0.6	2097.8	2033.0	307.8	12

morphologies in Fig. 10. In conclusion, 0.2Nb-MSS had the best corrosion resistance.

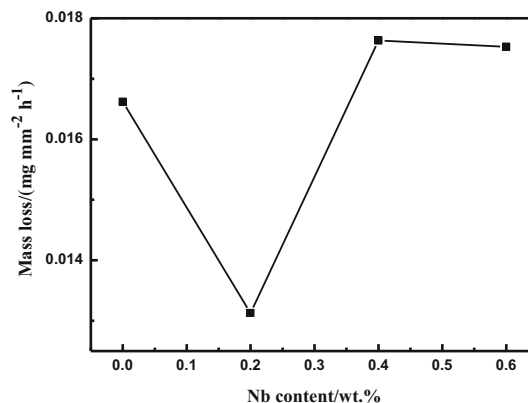


Fig. 11 Corrosion rates of samples after immersion corrosion test at room temperature for 12 h in 6 wt.% FeCl_3 solution

4 Conclusions

1. The addition of Nb can promote the carbide precipitation and change the composition of carbides. Nb element promotes the formation of Nb-rich carbide and inhibits Cr-rich carbide precipitation. At the same time, more addition of Nb element will transform the carbide from spherical-type to short rod-type and even the chain-type, lowering C content of matrix and hardness.

2. 0.2 wt.% Nb addition to MSS could maintain the hardness and improve the tensile strength (1714.1 MPa) with less ductile damage (reduced by 3.2%). But with the increase in Nb content, carbides gathered and transformed into chains and deteriorated mechanical properties such as the tensile strength and elongation at the same time.
3. Because of the inhibited effect on Cr-rich carbides precipitation by Nb addition, the corrosion resistance of 0.2Nb-MSS sample has been promoted. And a large amount of carbides cause carbon content to decrease to a critical minimum value required for nucleation of Fe–Cr phase.
4. The addition of Nb element of 0.2 wt.% is appropriate considering microstructure, mechanical properties and corrosion resistance.

References

- [1] E.H. Zhang, H.L. Zhang, *Coal Mine Machinery* 35 (2014) No.12, 16–18.
- [2] S.Y. Lu, K.F. Yao, Y.B. Chen, M.H. Wang, X. Liu, X.Y. Ge, *Electrochim. Acta* 165 (2015) 45–55.
- [3] P. Chen, X. Xiang, T.M. Shao, Y.Q. La, J.L. Li, *Appl. Surf. Sci.* 389 (2016) 361–368.
- [4] C.R. Chen, Y. Wang, H.G. Ou, Y.J. Lin, *Int. J. Fatigue* 92 (2016) 166–178.
- [5] M. Kiani, I. Gandikot, M. Rais-Rohani, K. Motoyam, J. Magnes. Alloy. 2 (2014) 99–108.
- [6] Y.X. Li, Z.G. Lin, A.Q. Jiang, G.L. Chen, *Mater. Des.* 24 (2003) 177–182.
- [7] R.C. Fan, M. Gao, Y.C. Ma, X.D. Zha, X.C. Hao, K. Liu, J. *Mater. Sci. Technol.* 28 (2012) 1059–1066.
- [8] X.P. Ma, L.J. Wang, B. Qin, C.M. Liu, S.V. Subramanian, *Mater. Des.* 34 (2012) 74–81.
- [9] F. Yang, J.F. Xu, A.J. Zhu, J. Gao, *Foundry Technol.* 32 (2011) 559–562.
- [10] H. Gwon, J.K. Kim, B. Jian, H. Mohrbacher, T. Song, S.K. Kim, B. De Cooman, *Mater. Sci. Eng. A* 711 (2018) 130–139.
- [11] X.P. Ma, L.J. Wang, C.M. Liu, S.V. Subramanian, *Mater. Sci. Eng. A* 528 (2011) 6812–6818.
- [12] L.L. Yang, *Hot Working Technol.* 44 (2015) No.18, 197–199.
- [13] M. Pavličková, D. Vojtěch, P. Novák, J. Gemperlová, A. Gemperle, N. Zárubová, P. Lejček, P. Jurčí, P. Stolař, *Mater. Sci. Eng. A* 356 (2003) 200–207.
- [14] M.A. Hamidzadeh, M. Meratian, M.M. Zahrani, *Mater. Sci. Eng. A* 556 (2012) 758–766.
- [15] Y. Gu, G.Y. Qiao, D.Y. Wu, B. Liao, F.R. Xiao, *Mater. Chem. Phys.* 183 (2016) 506–515.
- [16] S. Kheirandish, A. Noorian, *J. Iron Steel Res. Int.* 15 (2008) No.4, 61–66.
- [17] A. Noorian, S. Kheirandish, H. Saghafian, *Iran. J. Mater. Sci. Eng.* 7 (2010) No.2, 22–29.
- [18] J.W. Yang, W.S. Zhou, J.S. Lu, F. Yu, D. Xu, W.Q. Cao, *Iron and Steel* 50 (2015) No.7, 84–91.
- [19] C.W. Wu, J.X. Dong, M.C. Zhang, G.L. Wang, X.S. Xie, *Acta Metall. Sin. (Engl. Lett.)* 37 (2001) 1174–1178.
- [20] X.P. Ma, B. Labgeller, B. Gault, S. Subramanian, *Metall. Mater. Trans. A* 48 (2017) 2460–2471.
- [21] Y.Z. Shen, X.L. Zhou, T.T. Shi, X. Huang, Z.X. Shang, W.W. Liu, B. Ji, Z.Q. Xu, *Mater. Character.* 122 (2016) 113–123.
- [22] Y. Kang, W.M. Mao, Y.J. Chen, J. Jing, M. Cheng, *Mater. Sci. Eng. A* 677 (2016) 453–464.
- [23] X. Qi, H.H. Mao, Y.T. Yang, *Corros. Sci.* 120 (2017) 90–98.